

# Catalysis Science & Technology

Accepted Manuscript



This article can be cited before page numbers have been issued, to do this please use: J. Xu, Y. Gan, P. Hu, H. Zheng and B. Xue, *Catal. Sci. Technol.*, 2018, DOI: 10.1039/C8CY01688G.



This is an Accepted Manuscript, which has been through the Royal Society of Chemistry peer review process and has been accepted for publication.

Accepted Manuscripts are published online shortly after acceptance, before technical editing, formatting and proof reading. Using this free service, authors can make their results available to the community, in citable form, before we publish the edited article. We will replace this Accepted Manuscript with the edited and formatted Advance Article as soon as it is available.

You can find more information about Accepted Manuscripts in the [author guidelines](#).

Please note that technical editing may introduce minor changes to the text and/or graphics, which may alter content. The journal's standard [Terms & Conditions](#) and the ethical guidelines, outlined in our [author and reviewer resource centre](#), still apply. In no event shall the Royal Society of Chemistry be held responsible for any errors or omissions in this Accepted Manuscript or any consequences arising from the use of any information it contains.



Journal Name

ARTICLE

## Comprehensive insight into the support effect of graphitic carbon nitride for zinc halides in catalytic transformation of CO<sub>2</sub> to cyclic carbonates

Received 00th January 20xx,  
Accepted 00th January 20xx

DOI: 10.1039/x0xx00000x

www.rsc.org/

Jie Xu<sup>a,\*</sup>, Yu-Lin Gan<sup>a</sup>, Peng Hu<sup>a</sup>, Huan Zheng<sup>a</sup>, Bing Xue<sup>a,b,\*</sup>

Chemical fixation of CO<sub>2</sub> to high-valued chemicals is currently a significant research topic in both environment and chemistry, and cycloaddition of CO<sub>2</sub> with epoxides is regarded as a sustainable route for the manufacture of cyclic carbonates. The homogeneous catalysts including ionic liquid and organic metal complexes suffer from difficulty in catalyst-product separation despite their excellent catalytic activities. In this work, we utilized graphitic carbon nitride (g-C<sub>3</sub>N<sub>4</sub>) as a novel support to immobilize zinc halides (ZnX<sub>2</sub>) through a simple preparation method. Based on the detailed design in the synthesis of ZnX<sub>2</sub>/g-C<sub>3</sub>N<sub>4</sub>, the chemical bonding information of ZnX<sub>2</sub> on g-C<sub>3</sub>N<sub>4</sub> was comprehensively investigated by XPS and FT-IR techniques. In addition to activation of CO<sub>2</sub>, g-C<sub>3</sub>N<sub>4</sub> can anchor zinc halides via interaction between zinc and nitrogen, thereby effectively alleviating potential leaching of zinc halides. As heterogeneous catalysts, ZnX<sub>2</sub>/g-C<sub>3</sub>N<sub>4</sub> materials showed good catalytic activities in the cycloaddition reactions of CO<sub>2</sub> with propylene oxide. Furthermore, a wide range of epoxides can be converted to the corresponding cyclic carbonate with good selectivities (>93%) and moderate conversions (50–88%).

### 1. Introduction

The past decades have witnessed the drastically increasing emission of CO<sub>2</sub> as the main product of modern fossil-based energy production. CO<sub>2</sub> is believed to be primarily responsible for global warming and its associated climate change<sup>1-3</sup>. Alternatively, CO<sub>2</sub> is a nontoxic, abundant, and sustainable C1 feedstock for organic synthesis. In this sense, transformation of CO<sub>2</sub> to the high-valued chemicals could not only alleviate the continuous emission of CO<sub>2</sub> but also provide a renewable and promising strategy to supplement conventional fossil-based resource<sup>4,5</sup>. Among numerous examples of chemical fixation of CO<sub>2</sub>, the synthesis of cyclic carbonates based on the cycloaddition of CO<sub>2</sub> with epoxides have received tremendous attention<sup>6</sup>, as cyclic carbonates are of important commodity chemicals, which are extensively applied as polar solvents, fuel additives, electrolytes, and building blocks in the manufacture of pharmaceutical and other fine chemicals<sup>7,8</sup>.

Due to its low reactivity and thermal stability, the transformation of CO<sub>2</sub> always demands a principal step in activating CO<sub>2</sub> molecules. Wherein, the kernel of the procedure is to develop and research a robust catalyst. Up to now, the

most efficient catalysts proposed for the cycloaddition of CO<sub>2</sub> with epoxides have been confined to several materials including ionic liquids<sup>3,7,9,10</sup>, organic metal complexes<sup>11,12</sup>, quaternary ammonium<sup>13,14</sup>, etc. Unfortunately, their intrinsically homogeneous nature in the reaction systems inevitably hinders them from industrial implementation<sup>3,8</sup>. From the aspect of catalytic mechanism, it is commonly recognized that basic sites and Lewis acid (e.g. zinc halide) are two key components to promote the cycloaddition of CO<sub>2</sub> with epoxide<sup>15-19</sup>. Basic sites on the catalyst are able to adsorb and then activate CO<sub>2</sub> while Lewis acid could stimulate the ring-opening of epoxides. In the light of this fact, a lot of bicomponent catalysts, including DBU/benzyl bromide<sup>20</sup>, melamine-ZnI<sub>2</sub><sup>21</sup>, Zn-SBA-15/KI<sup>22</sup>, ZnCl<sub>2</sub>/phosphonium halide<sup>16</sup>, ZnBr<sub>2</sub>-Ph<sub>4</sub>PI<sup>23</sup>, etc., have been developed. However, it should be pointed out that most of them belong to homogeneous catalysts, being confronted with disadvantage in catalyst recovery and product purification. Additionally, several catalysts also suffer from leaching problem of active species.

Very recently, as a fascinating functional material, graphitic carbon nitride (g-C<sub>3</sub>N<sub>4</sub>) has received wide interest in a variety of research fields including photocatalysis<sup>24-26</sup>, thermal catalysis<sup>17,27-30</sup>, fuel cells<sup>31</sup>, etc. In terms of chemical structure, g-C<sub>3</sub>N<sub>4</sub> is built by two-dimensional graphite-like sheets containing conjugated tri-s-triazine units<sup>24,32,33</sup>. Especially at the edges of graphitic layers, there exist abundant uncondensed amino groups, which enable g-C<sub>3</sub>N<sub>4</sub> as a typical solid base<sup>17,34,35</sup>. Antonietti et al have found g-C<sub>3</sub>N<sub>4</sub> could adsorb and activate CO<sub>2</sub> molecules by means of its uncondensed amines<sup>36</sup>. Park et al have revealed that g-C<sub>3</sub>N<sub>4</sub> materials could catalyze

<sup>a</sup> Jiangsu Key Laboratory of Advanced Catalytic Materials and Technology, School of Petrochemical Engineering, Changzhou University, Gehu Middle Road 21, Changzhou, Jiangsu 213164, PR China. E-mail: [shine6832@163.com](mailto:shine6832@163.com); Tel.: +86-519-86330135; Fax.: +86-519-86330135

<sup>b</sup> State Key Laboratory of Chemical Resource Engineering, Beijing University of Chemical Technology, Beijing 100029, PR China. E-mail: [xuebing\\_cn@163.com](mailto:xuebing_cn@163.com)

† Electronic Supplementary Information (ESI) available: [details of any supplementary information available should be included here]. See DOI: 10.1039/x0xx00000x

cycloaddition of CO<sub>2</sub> with epoxides, and other CO<sub>2</sub>-involved processes<sup>37</sup>. Most recently, some groups including ours have also reported cycloaddition of CO<sub>2</sub> reactions catalyzed by decorated and/or supported mesoporous g-C<sub>3</sub>N<sub>4</sub> materials<sup>17,18,35,38-41</sup>. Despite these advances, the preparation of such reported g-C<sub>3</sub>N<sub>4</sub> materials are indeed quite complicated. In addition to the above basic property, the rich nitrogen atoms in carbon skeleton also endow g-C<sub>3</sub>N<sub>4</sub> with a potential like chlorophyll, hemin and other macrocyclic scaffolds, to include and anchor metal elements<sup>25,42</sup>. The recent work reported by Vinu, Wang and several groups revealed that g-C<sub>3</sub>N<sub>4</sub> could well disperse Au<sup>43</sup>, Fe<sup>44,45</sup>, Zn<sup>25,46</sup>, V<sup>29</sup>, Cu<sup>47</sup>, and other metals<sup>42</sup>.

Since g-C<sub>3</sub>N<sub>4</sub> possesses inherent basic characters and promising capability of metal inclusion in its matrix, in this work, a series of zinc halides supported on g-C<sub>3</sub>N<sub>4</sub> were synthesized by means of simple pyrolysis of dicyandiamide, followed by wet impregnation of zinc halides. The bonding states of zinc and halogen elements on the surface of g-C<sub>3</sub>N<sub>4</sub>, depending on the heating temperature of the composites, were comprehensively investigated. The nitrogen species of g-C<sub>3</sub>N<sub>4</sub> interact with zinc, rendering it steadily anchored on g-C<sub>3</sub>N<sub>4</sub> and thus effectively inhibiting possible leaching of zinc halide. The combination of zinc halides and g-C<sub>3</sub>N<sub>4</sub> promotes the cycloaddition of CO<sub>2</sub> to cyclic carbonates. Moreover, according to the characterization results, a possible catalytic mechanism is proposed.

## 2. Experimental

### 2.1. MATERIAL PREPARATION

The g-C<sub>3</sub>N<sub>4</sub> material was synthesized using dicyandiamide (DCDA) as a precursor. In brief, 6 g of DCDA was added into a ceramic crucible with a cover, heated with a ramping rate of 3 °C min<sup>-1</sup> to 550 °C, and then tempered at this temperature for another 3 h. The resultant g-C<sub>3</sub>N<sub>4</sub> was ca. 2.1 g.

The g-C<sub>3</sub>N<sub>4</sub> powder (1 g) was suspended into 20 mL of ethanol containing zinc halide (ZnX<sub>2</sub>, X = Cl/Br/I), stirred vigorously for 2 h, and dried at 50 °C. The as-synthesized yellow solid was placed into a tubular furnace with the flow of nitrogen (10–20 mL min<sup>-1</sup>), heated with a rate of 2 °C min<sup>-1</sup> to a desired temperature, and then hold for another 3 h. The obtained material was labeled as *x*ZnX<sub>2</sub>/g-C<sub>3</sub>N<sub>4</sub>-*T*, where *x* represented the molar amount (mmol) of zinc halide, and *T* indicated the heating temperatures. Unless other specified, *x* and *T* were 1 mmol and 400 °C, respectively.

NH<sub>4</sub>X/g-C<sub>3</sub>N<sub>4</sub> and ZnO/g-C<sub>3</sub>N<sub>4</sub> samples were synthesized by the same method above yet using ammonium halide and Zn(NO<sub>3</sub>)<sub>2</sub>, respectively

### 2.2. SAMPLE CHARACTERIZATION

Nitrogen adsorption–desorption isotherms were measured at –196 °C using an ASAP 2020 (Micromeritics) porosimeter. Prior to the measurement, each sample was outgassed at 150 °C for at least 4 h. The specific surface area of the sample was calculated using the BET method.

The powder X-ray diffraction (XRD) patterns were recorded with a Rigaku D/max 2500 PC X-ray diffractometer

equipped with a graphite monochromator using Ni-filtered Cu-Kα (λ = 0.154 nm) radiation.

Fourier transform infrared (FT-IR) spectra in transmission mode were analyzed on a Tensor 27 (Bruker) spectrometer by averaging 64 scans with a resolution of 4 cm<sup>-1</sup>. The spectra were recorded under ambient condition using the KBr self-supported pellet technique.

UV–vis diffuse reflectance spectra (DRS) were measured on a UV-3600 (Shimizu) spectrophotometer under ambient condition using BaSO<sub>4</sub> as the reference.

X-ray photoelectron spectroscopy (XPS) measurements were performed using a Perkin–Elmer PHI 5000C instrument with a monochromatized Mg K<sub>α</sub> radiation source (200 W).

Propylene oxide temperature-programmed desorption (PO-TPD) was analyzed on a ChemBET-3000 station (Quantachrome). Each sample (200 mg, crushed into 40–60 meshes) was pretreated at 200 °C for 1 h under He flow, and then cooled down to 50 °C, followed by purge of PO-containing helium gas (PO saturated gas under 40 °C) for 0.5 h. Afterwards, the sample was swept with He (60 mL min<sup>-1</sup>) for 0.5 h, and then heated a rate of 10 °C min<sup>-1</sup> to 500 °C.

CO<sub>2</sub>- and NH<sub>3</sub>-TPD experiments were performed in the same way to PO-TPD, expect using CO<sub>2</sub> and NH<sub>3</sub> as adsorbates.

200 mg of ZnBr<sub>2</sub>/g-C<sub>3</sub>N<sub>4</sub> was added into a solution containing 8 mL of PO and 2 mL of DMF. The mixture was heated at 140 °C for ca. 6 h under stirring. After that, the liquid phase was collected and then analyzed by inductively coupled plasma atomic emission spectroscopy (ICP-AES, Vista-AX, Varian) to determine the concentration of Zn<sup>2+</sup>.

### 2.3. CATALYTIC TEST

Cycloaddition reaction of CO<sub>2</sub> with propylene oxide (PO) to propylene carbonate (PC) was performed in a stainless steel autoclave (80 mL). PO (8 mL, 115 mmol), *N,N*-dimethyl formamide (DMF, 2 mL), and 0.2 g of catalyst were added into the reactor, which was then pressurized with CO<sub>2</sub> to 2.0 MPa. The reaction was carried out at 140 °C under vigorous stirring for 6 h. After completion of the reaction, the liquid-phase mixture was separated by centrifugation, and firstly analyzed by a gas chromatography-mass spectrometer (GC-MS, GCMS-QP2010, Shimadzu) to qualitatively confirm the products. The quantitative analysis of the reaction mixture was determined by a gas chromatography (GC) equipped with an SE-54 capillary column and FID (See the supporting information for detailed profiles of GC). The liquid mixture contained PO, PC, and 1,2-propylene glycol (PG) as the byproduct derived from hydrolysis of PO with trace H<sub>2</sub>O. The carbon balance was nearly 100%. PO conversion and selectivity to PC were calculated based on an area-normalization method of GC, and the corresponding calculation equations are as follows:

$$\text{Conv.} = \frac{A_{\text{PC}} \times f_{\text{PC}} + A_{\text{PG}} \times f_{\text{PG}}}{A_{\text{PO}} + A_{\text{PC}} \times f_{\text{PC}} + A_{\text{PG}} \times f_{\text{PG}}}, \quad \text{Sel.} = \frac{A_{\text{PC}} \times f_{\text{PC}}}{A_{\text{PC}} \times f_{\text{PC}} + A_{\text{PG}} \times f_{\text{PG}}}$$

where *A*, and *f* are the peak areas of GC, and response factor for each product.

In the reaction cases involving ethylene carbonate (EC), PC, and 1,2-butylene carbonate (BC) as products, the liquid-phase mixture was separated by centrifugation. After

elimination of DMF under vacuum and further purification by column chromatography with ethyl acetate–petroleum ether as the eluent, the resultant products were analyzed by  $^1\text{H}$  NMR and  $^{13}\text{C}$  NMR spectroscopy.

The quasi-TOF (mass of synthesized PC per gram catalyst per hour) for each catalyst was calculated as follows:

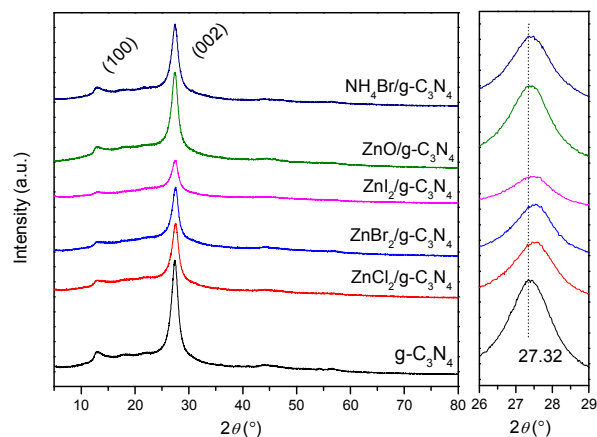
$$\text{TOF} = \frac{m_{\text{PC}}}{W_{\text{catal.}} \times t} = \frac{n_{\text{PO}} \times \text{Yield}\% \times M_{\text{PC}}}{W_{\text{catal.}} \times t}$$

where  $n_{\text{PO}}$ ,  $M_{\text{PC}}$ ,  $t$ , and  $W_{\text{catal.}}$  were the molar amount (mol) of PO, formula weight ( $\text{g mol}^{-1}$ ) of PC, reaction time (h), and the mass of overall catalyst (g), respectively.

### 3. Results

#### 3.1. Structure characterization

The XRD patterns of the bare and the doped  $\text{g-C}_3\text{N}_4$  materials are shown in **Fig. 1**. All the patterns exhibit primary diffraction lines at ca.  $2\theta = 27.3^\circ$ , corresponding to the characteristic interplanar stacking ( $d = 0.34$  nm) of graphitic materials, i.e. (002) planes of  $\text{g-C}_3\text{N}_4$ <sup>32,42</sup>. Moreover, a relatively weak diffraction peak can be also found at ca.  $2\theta = 13^\circ$  for each sample, which is attributed to in-plane packing motif, i.e. (100) plane ( $d = 0.67$  nm)<sup>32,48</sup>. Compared with that of the pristine  $\text{g-C}_3\text{N}_4$ , the intensities of both (002) and (100) become much lower. This means that, after the incorporation of dopant into  $\text{g-C}_3\text{N}_4$ , the crystallinity of  $\text{g-C}_3\text{N}_4$  weakens; the similar phenomena have been previously reported in the work involving  $\text{g-C}_3\text{N}_4$  materials doped with K<sup>49</sup>, Fe<sup>45</sup>, Zn<sup>25,46</sup>, etc.

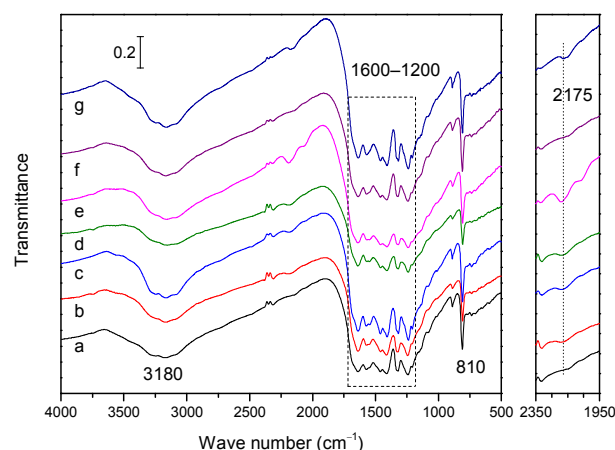


**Fig. 1** XRD patterns of  $\text{g-C}_3\text{N}_4$ ,  $\text{ZnX}_2/\text{g-C}_3\text{N}_4$ ,  $\text{NH}_4\text{Br}/\text{g-C}_3\text{N}_4$  and  $\text{ZnO}/\text{g-C}_3\text{N}_4$  materials.

**Table 1** Surface areas of  $\text{g-C}_3\text{N}_4$ ,  $\text{ZnX}_2/\text{g-C}_3\text{N}_4$ ,  $\text{NH}_4\text{Br}/\text{g-C}_3\text{N}_4$ , and  $\text{ZnO}/\text{g-C}_3\text{N}_4$  materials.

Sample	$S_{\text{BET}}$ ( $\text{m}^2 \text{g}^{-1}$ )
$\text{g-C}_3\text{N}_4$	14
$\text{ZnCl}_2/\text{g-C}_3\text{N}_4$	8
$\text{ZnBr}_2/\text{g-C}_3\text{N}_4$	6
$\text{ZnI}_2/\text{g-C}_3\text{N}_4$	10
$\text{ZnO}/\text{g-C}_3\text{N}_4$	10
$\text{NH}_4\text{Br}/\text{g-C}_3\text{N}_4$	21

It is of interest to be observed that, for the  $\text{g-C}_3\text{N}_4$  materials doped with zinc halides, the intensity order related to (002) plane is  $\text{Cl} > \text{Br} > \text{I}$ . The detailed diffraction patterns in the range of  $2\theta = 26\text{--}29^\circ$  are also given in **Fig. 1**. The diffraction peaks of the  $\text{ZnX}_2/\text{g-C}_3\text{N}_4$  samples are moved towards to higher  $2\theta$  values in comparison with that of  $\text{g-C}_3\text{N}_4$ , whereas there is no significant shift in the cases of  $\text{NH}_4\text{Br}/\text{g-C}_3\text{N}_4$  and  $\text{ZnO}/\text{g-C}_3\text{N}_4$ . The above shift evidences the shrinkage of interplanar spacing of  $\text{g-C}_3\text{N}_4$  in the  $\text{ZnX}_2/\text{g-C}_3\text{N}_4$  materials, which however has not been discovered in the XRD patterns of  $\text{NH}_4\text{Br}/\text{g-C}_3\text{N}_4$  and  $\text{ZnO}/\text{g-C}_3\text{N}_4$ . The distinction suggests that the shrinkage of graphitic interlayers occurs only if the zinc and halides exist together. The surface areas of the pristine  $\text{g-C}_3\text{N}_4$  and its doped materials are listed in **Table 1**. The surface area of  $\text{g-C}_3\text{N}_4$  is  $14 \text{ m}^2 \text{g}^{-1}$ , while the  $\text{ZnX}_2/\text{g-C}_3\text{N}_4$  materials have lower surface area. By contrast,  $\text{NH}_4\text{Br}/\text{g-C}_3\text{N}_4$  possesses larger surface area ( $21 \text{ m}^2 \text{g}^{-1}$ ) than  $\text{g-C}_3\text{N}_4$ . This might be due to the decomposition of  $\text{NH}_4\text{Br}$ , which creates many interparticle voids in  $\text{g-C}_3\text{N}_4$ .



**Fig. 2** FT-IR spectra of  $\text{g-C}_3\text{N}_4$  (a),  $\text{ZnCl}_2/\text{g-C}_3\text{N}_4$  (b),  $\text{ZnBr}_2/\text{g-C}_3\text{N}_4$  (c),  $\text{ZnI}_2/\text{g-C}_3\text{N}_4$  (d),  $\text{ZnO}/\text{g-C}_3\text{N}_4$  (e),  $\text{NH}_4\text{Br}/\text{g-C}_3\text{N}_4$  (f), and  $\text{KBr}/\text{g-C}_3\text{N}_4$  (g) materials.

FT-IR spectra of the materials are depicted in **Fig. 2**. The supported  $\text{g-C}_3\text{N}_4$  samples demonstrate similar spectra to the bare  $\text{g-C}_3\text{N}_4$ . The broad bands centered at  $3180 \text{ cm}^{-1}$  are assigned to the N–H groups (terminal amino groups at the edge of graphitic sheets) and H–O derived from adsorbed water<sup>35</sup>, and the multiple transmission bands ranging from  $1600$  to  $1200 \text{ cm}^{-1}$  are indicative of aromatic nitrogen-containing heterocycles<sup>48</sup>. The sharp peaks at  $810 \text{ cm}^{-1}$  correspond to the breathing mode of the graphitic layers constituted by conjugated triazine (or tri-*s*-triazine) units, which are regarded as the elementary building blocks of  $\text{g-C}_3\text{N}_4$ <sup>50,51</sup>. Obviously, the induction of  $\text{ZnX}_2$  and other compounds has not altered the overall chemical functionalities of  $\text{g-C}_3\text{N}_4$ . Despite the analogy, a low-intensity band at ca.  $2175 \text{ cm}^{-1}$  is identified in the spectra of  $\text{ZnX}_2/\text{g-C}_3\text{N}_4$  and  $\text{ZnO}/\text{g-C}_3\text{N}_4$ , which is however absent in those of  $\text{g-C}_3\text{N}_4$  and  $\text{NH}_4\text{Br}/\text{g-C}_3\text{N}_4$ . The unique signal is ascribed to the azide group due to the existence of Zn–N bonding<sup>46</sup>. Moreover, a further comparison witnesses that, among the three  $\text{ZnX}_2/\text{g-C}_3\text{N}_4$  samples,  $\text{ZnI}_2/\text{g-C}_3\text{N}_4$  possesses

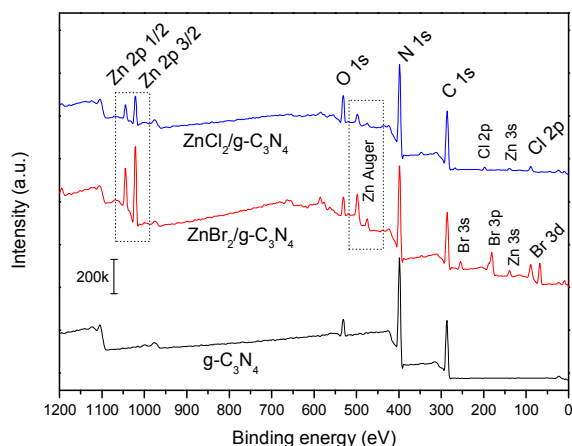


## ARTICLE

## Journal Name

the highest intensity in terms of the band about Zn–N group, followed by ZnBr<sub>2</sub>/g-C<sub>3</sub>N<sub>4</sub> and ZnCl<sub>2</sub>/g-C<sub>3</sub>N<sub>4</sub>. The finding agrees well with the order obtained in the above XRD patterns. As for the FT-IR spectrum of KBr/g-C<sub>3</sub>N<sub>4</sub>, the emergence of the azide group (K–N=N) <sup>49</sup> is also identified at ca. 2145 cm<sup>-1</sup>. The above FT-IR characterization results reveal that the loading of zinc halides has not modified the main chemical functionalities of g-C<sub>3</sub>N<sub>4</sub>, whereas Zn has reacted with g-C<sub>3</sub>N<sub>4</sub> and inserted into the skeleton thereof.

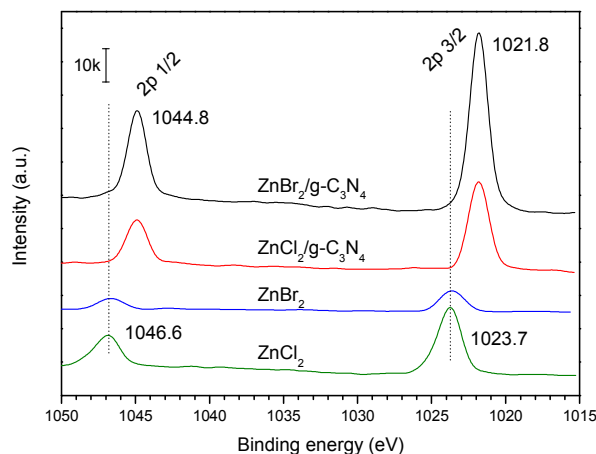
The chemical environment of the materials was further analyzed by XPS. The major elements detected in g-C<sub>3</sub>N<sub>4</sub> are carbon, nitrogen, and oxygen (**Fig. 3**); the chemical formula calculated by means of the XPS survey is C<sub>0.92</sub>N<sub>0.10</sub>. Therein, the oxygen is mainly due to the adsorbed water molecule. The presence of zinc signals could be clearly observed in the spectra of ZnCl<sub>2</sub>/g-C<sub>3</sub>N<sub>4</sub> and ZnBr<sub>2</sub>/g-C<sub>3</sub>N<sub>4</sub>; the molar ratios of carbon to nitrogen of the two samples are 1.17:1 and 1.06:1, respectively. Furthermore, the molar ratios of Zn to halide in the cases of ZnCl<sub>2</sub>/g-C<sub>3</sub>N<sub>4</sub> and ZnBr<sub>2</sub>/g-C<sub>3</sub>N<sub>4</sub> are 2.53:1 and 1.08:1. In our previous work <sup>34,38</sup>, we discovered there was an interaction of zinc halide and g-C<sub>3</sub>N<sub>4</sub> under high temperature. That is, a certain amount of halide reacted with the uncondensed terminal amines of g-C<sub>3</sub>N<sub>4</sub>, generating hydrogen halide and ammonium halide. Wherein, HCl was more volatile than HBr, leading to less concentration of halogen elements reserving in ZnCl<sub>2</sub>/g-C<sub>3</sub>N<sub>4</sub> than that gained in ZnBr<sub>2</sub>/g-C<sub>3</sub>N<sub>4</sub>. Nevertheless, it is worth noting that, there remain partial halide species as counter ions to neutralize zinc cation in the composites <sup>46,52</sup>.



**Fig. 3** XPS survey of g-C<sub>3</sub>N<sub>4</sub>, ZnCl<sub>2</sub>/g-C<sub>3</sub>N<sub>4</sub>, and ZnBr<sub>2</sub>/g-C<sub>3</sub>N<sub>4</sub> samples.

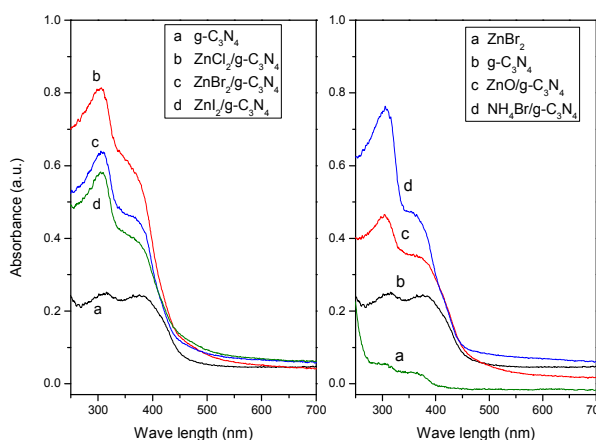
To gain an insight of the bonding state of Zn, the fine spectra of ZnCl<sub>2</sub>/g-C<sub>3</sub>N<sub>4</sub> and ZnBr<sub>2</sub>/g-C<sub>3</sub>N<sub>4</sub> were recorded (**Fig. 4**). Both the two spectra present two pronounced peaks at binding energies of 1044.8 and 1021.8 eV, indexed as the signals of Zn 2p 1/2 and 3/2 orbits <sup>46,53,54</sup>, respectively. For purpose of comparison, the spectra of pure ZnBr<sub>2</sub> and ZnCl<sub>2</sub> compounds are also provided in **Fig. 4**; the corresponding Zn 2p lines appear at 1046.6 and 1023.7 eV, quite higher than the values of the two composites. On the other hand, the binding energy for 2p 3/2 line of metallic zinc is about 1020 eV <sup>55</sup>. This confirms

that the valence states of zinc cations in the supported materials are lower than +2, therefore manifesting the interaction between Zn and nitrogen of g-C<sub>3</sub>N<sub>4</sub>.



**Fig. 4** Zn 2p XP spectra of ZnCl<sub>2</sub>, ZnBr<sub>2</sub>, ZnCl<sub>2</sub>/g-C<sub>3</sub>N<sub>4</sub>, and ZnBr<sub>2</sub>/g-C<sub>3</sub>N<sub>4</sub>.

UV–vis diffuse spectroscopy is usually applied to probe the effect of metal incorporation on the host structure. As indicated in **Fig. 5**, the spectrum of g-C<sub>3</sub>N<sub>4</sub> shows a distinct absorption peak in UV region, which is derived from the bandgap between HOMO and LUMO of polymeric triazine units <sup>24,41</sup>. After the loading of zinc halides, the major absorption is enhanced and meanwhile is moved towards longer wavelength. According to Wang et al <sup>25,42</sup>, the shift also observed in the spectra of Zn-containing g-C<sub>3</sub>N<sub>4</sub> materials results from the d–p repulsion of N 2p and Zn 3d orbits. Combining the analytic results of FT-IR, XPS and UV–vis techniques, it can be concluded that for the three supported zinc halides, the zinc species existed in the forms of coordinative state with nitrogen of g-C<sub>3</sub>N<sub>4</sub> rather than the pure compound. Simultaneously, the low-valence zinc cations are neutralized by a small portion of halides (discussed below).



**Fig. 5** UV–vis diffuse reflection spectra of g-C<sub>3</sub>N<sub>4</sub>, ZnX<sub>2</sub>/g-C<sub>3</sub>N<sub>4</sub>, NH<sub>4</sub>Br/g-C<sub>3</sub>N<sub>4</sub> and ZnO/g-C<sub>3</sub>N<sub>4</sub> materials.

### 3.2. Catalyst evaluation

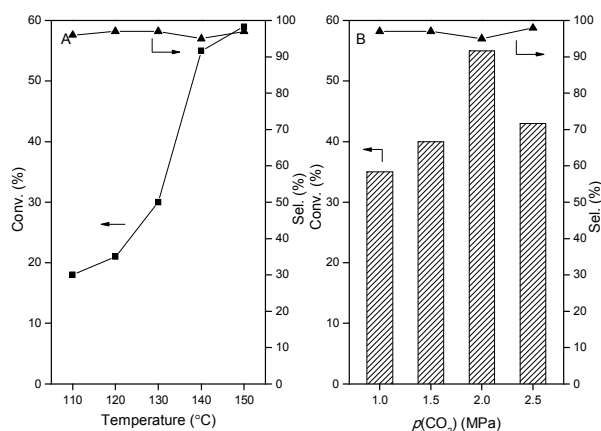
Initially, the cycloaddition reaction of CO<sub>2</sub> with PO was tested in the presence of 0.2 g of g-C<sub>3</sub>N<sub>4</sub> at 140 °C. As listed in **Table 2**, after 6 h of reaction time, only 3% of PO was converted (entry 1). Meanwhile, the resultant products consist of PC and PG; the latter is originated from hydrolysis of PO. Upon using ZnCl<sub>2</sub> as a catalyst, the catalytic conversion of PO reaches up to 99% and the selectivity to the target PC is 98% (entry 2). Likewise, remarkably high yields of PC have also been achieved in the cases of ZnBr<sub>2</sub> and ZnI<sub>2</sub> (entries 3–4) under the same reaction conditions. Notwithstanding so high catalytic activities, as stated above, the zinc halides are well dissolved in the liquid phase. After the reaction, it is inconvenient to separate the homogeneous catalyst from the reaction system. On the other hand, among the three ZnX<sub>2</sub>/g-C<sub>3</sub>N<sub>4</sub> materials (entries 5–7), ZnBr<sub>2</sub>/g-C<sub>3</sub>N<sub>4</sub> shows superior activity to ZnCl<sub>2</sub>/g-C<sub>3</sub>N<sub>4</sub> and ZnI<sub>2</sub>/g-C<sub>3</sub>N<sub>4</sub>. The PO conversion and PC selectivity are 55% and 95%, respectively. The catalytic performance of ZnO/g-C<sub>3</sub>N<sub>4</sub> using Zn(NO<sub>3</sub>)<sub>2</sub> as a precursor has also been listed in **Table 2**; the corresponding PO conversion is only 19%.

**Table 2** Catalytic performances of various catalysts in cycloaddition of CO<sub>2</sub> with PO to PC<sup>a</sup>.

Entry	Catalyst	Conv. (%)	Sel. (%)	Yield (%)
1	g-C <sub>3</sub> N <sub>4</sub>	3	75	2
2 <sup>b</sup>	ZnCl <sub>2</sub>	99	98	97
3 <sup>b</sup>	ZnBr <sub>2</sub>	98	99	97
4 <sup>b</sup>	ZnI <sub>2</sub>	99	99	98
5	ZnCl <sub>2</sub> /g-C <sub>3</sub> N <sub>4</sub>	32	95	30
6	ZnBr <sub>2</sub> /g-C <sub>3</sub> N <sub>4</sub>	55	95	52
7	ZnI <sub>2</sub> /g-C <sub>3</sub> N <sub>4</sub>	36	97	35
8	ZnO/g-C <sub>3</sub> N <sub>4</sub>	19	97	18
9	NH <sub>4</sub> Cl/g-C <sub>3</sub> N <sub>4</sub>	11	92	10
10	NH <sub>4</sub> Br/g-C <sub>3</sub> N <sub>4</sub>	30	96	29
11	NH <sub>4</sub> I/g-C <sub>3</sub> N <sub>4</sub>	14	99	14
12 <sup>c</sup>	ZnBr <sub>2</sub> /g-C <sub>3</sub> N <sub>4</sub>	39	95	37
13	0.5ZnBr <sub>2</sub> /g-C <sub>3</sub> N <sub>4</sub>	25	93	23
14	1.5ZnBr <sub>2</sub> /g-C <sub>3</sub> N <sub>4</sub>	54	97	52

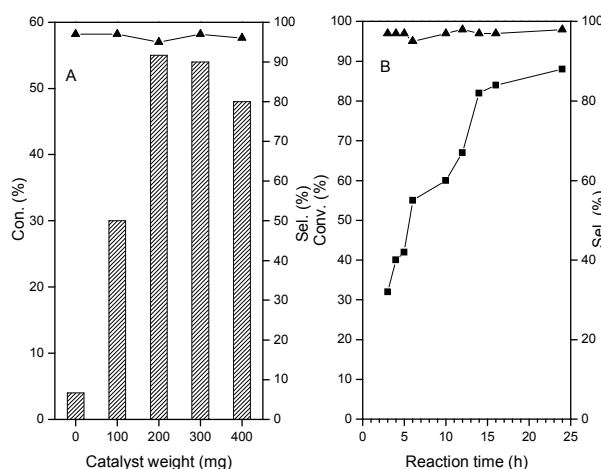
<sup>a</sup> Reaction conditions: 8 mL of PO, 2 mL of DMF, *W*<sub>catal.</sub> = 0.2 g, *T* = 140 °C, *t* = 6 h. <sup>b</sup> 0.2 mmol of ZnX<sub>2</sub>. <sup>c</sup> 8 mL PO without DMF.

Moreover, we have also evaluated the catalytic activities of various NH<sub>4</sub>X/g-C<sub>3</sub>N<sub>4</sub> materials for the cycloaddition reactions of CO<sub>2</sub> with PO. Like the order found in the abovementioned ZnX<sub>2</sub>/g-C<sub>3</sub>N<sub>4</sub> catalysts, the maximum PC yield (29%) is obtained in NH<sub>4</sub>Br/g-C<sub>3</sub>N<sub>4</sub> among the three NH<sub>4</sub>X/g-C<sub>3</sub>N<sub>4</sub> (entries 9–11). More importantly, through a detailed comparison of entries 6, 8 and 10, it can be found that the high catalytic activity of ZnBr<sub>2</sub>/g-C<sub>3</sub>N<sub>4</sub> indeed relies on the combination of both zinc and bromide. In other words, there is an apparent synergy of zinc and bromide in the catalytic reactions (discussed below). Furthermore, the catalytic performance in the absence of the DMF solvent was also evaluated under the identical reaction conditions, and the resultant conversion of PO is 39%, along with a selectivity to PC of 96% (entry 12). It is clear that DMF is also capable to promote the catalytic process, mainly owing to its basic property that facilitates to adsorb and activate CO<sub>2</sub> molecules<sup>38,56,57</sup>.



**Fig. 6** Effects of the reaction temperature (A) and CO<sub>2</sub> pressure (B) on the catalytic performances. Reaction conditions: 8 mL of PO, 2 mL of DMF, 0.2 g of ZnBr<sub>2</sub>/g-C<sub>3</sub>N<sub>4</sub>, *t* = 6 h, *p*(CO<sub>2</sub>) = 2.0 MPa (A), and *T* = 140 °C (B).

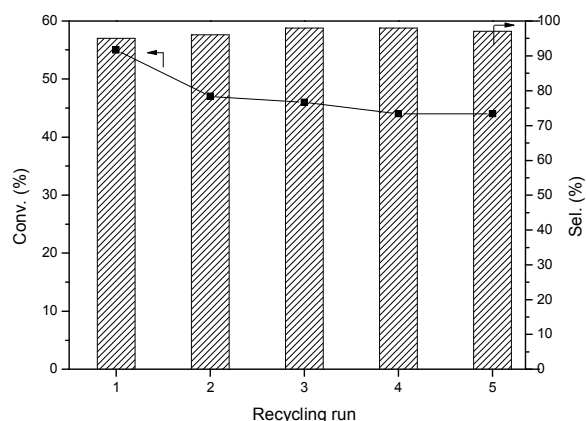
The influences of reaction conditions on catalytic results were subsequently studied. Using ZnBr<sub>2</sub>/g-C<sub>3</sub>N<sub>4</sub> as a representative catalyst, as the reaction conditions are elevated from 110 to 140 °C, the PO conversion increases progressively (**Fig. 6A**). At 150 °C, the conversion is 59%, slightly higher than the value obtained at 140 °C. The catalytic reaction is also sensitive to the pressure of CO<sub>2</sub> (**Fig. 6B**). The PO conversion increases gradually with the increment of the CO<sub>2</sub> pressure. However, adopting higher pressure would result in a dramatic decline of catalytic productivity. This phenomenon has been widely reported in the cycloaddition reactions employing other catalyst systems<sup>8,19,56,58</sup>. One probable explanation is that under excessively high pressure of CO<sub>2</sub>, much more acidic CO<sub>2</sub> molecules dissolve in basic PO liquid, further transforming into CO<sub>2</sub>-PO complexes<sup>58,59</sup>. The formation of such species deteriorates the reactivity of PO, therefore resulting in the decrease of PC yield.



**Fig. 7** Effects of the catalyst weight (A) and reaction time (B) on the catalytic performances. Reaction conditions: 8 mL of PO, 2 mL of DMF, *p*(CO<sub>2</sub>) = 2.0 MPa, *T* = 140 °C, *t* = 6 h (A), and 0.2 g of ZnBr<sub>2</sub>/g-C<sub>3</sub>N<sub>4</sub> (B).

The reactions using various amounts of catalyst have also been performed, and the resultant catalytic performance is given in **Fig. 7A**. Using much more catalyst could bring out a distinct enhancement of catalytic conversion. Nonetheless, as the catalyst weight is higher than 200 mg, the conversion shows an unfavorable decrease. This might be due to poor dispersion of catalyst solid in the reaction system, thereafter provoking limited mass transfer between the actives and reactants<sup>60</sup>. Additionally, the catalytic behavior within a long period of reaction has also been examined (**Fig. 7B**). As the reaction is prolonged to 14 h or longer, a very high catalytic conversion (>80%) can also be achieved over ZnBr<sub>2</sub>/g-C<sub>3</sub>N<sub>4</sub>.


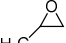



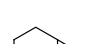
Recyclability is another important issue to evaluate a heterogeneous catalyst. After each catalytic run, the ZnBr<sub>2</sub>/g-C<sub>3</sub>N<sub>4</sub> catalyst was rinsed with ethanol and then used for its subsequent cycle. The resultant catalytic performances are depicted in **Fig. 8**. After the first test, the PO conversion was slightly decreased to 47%, whereas the catalytic activity remains stable within the subsequent several runs. We conjecture that a small amount of ZnBr<sub>2</sub> has not been steadily anchored on g-C<sub>3</sub>N<sub>4</sub>, therein leading to a partial leaching of ZnBr<sub>2</sub> from the catalyst. Since the catalytic reaction was performed under the polar solvent of DMF, to check on the possible dissolution of Zn<sup>2+</sup> of ZnBr<sub>2</sub>/g-C<sub>3</sub>N<sub>4</sub> into DMF, we performed a tentative test by adding 200 mg of ZnBr<sub>2</sub>/g-C<sub>3</sub>N<sub>4</sub> into 10 mL of reaction solution (the detailed operation is described in Section 2.2). The resultant concentration of Zn<sup>2+</sup> was ca. 2.15 mmol L<sup>-1</sup>. If all the Zn<sup>2+</sup> cations of the 200-mg catalyst (corresponding to ca. 0.2 mmol of ZnBr<sub>2</sub>) were leached into the liquid phase of reaction, the concentration of Zn<sup>2+</sup> would be up to ca. 20 mmol L<sup>-1</sup>. It is apparent that most of Zn<sup>2+</sup> species have been well reserved on the ZnBr<sub>2</sub>/g-C<sub>3</sub>N<sub>4</sub> composite. Moreover, XRD and FT-IR were applied again to analyze the spent catalyst subjected to five catalytic tests. As presented in **Fig. S1**, the recycled catalyst has almost identical chemical functionalities and structure to the fresh one, indicating the ZnBr<sub>2</sub>/g-C<sub>3</sub>N<sub>4</sub> material is relatively stable as a heterogeneous catalyst.



**Fig. 8** Recycling tests of cycloaddition of CO<sub>2</sub> with PO to PC catalyzed by ZnBr<sub>2</sub>/g-C<sub>3</sub>N<sub>4</sub>. Reaction conditions: 8 mL of PO, 2 mL of DMF,  $p(\text{CO}_2) = 2.0$  MPa,  $T = 140$  °C,  $t = 6$  h, and  $W_{\text{catal.}} = 0.2$  g.

Besides the recycling evaluation, to investigate the versatile applicability of ZnBr<sub>2</sub>/g-C<sub>3</sub>N<sub>4</sub>, we have also performed several cycloaddition reactions adopting various epoxides. As shown in **Table 3**, under the same reaction conditions, the most reactive substrate is epichlorohydrin (ECH), the conversion and selectivity to the target molecular (chloroethylene carbonate) are 88% and 94%, respectively. The by-product (as well as found in other entries of **Table 3**) is mainly the hydrolyzed compound of ECH due to the contacting with residual water under high reaction temperature. In fact, these byproducts have also been widely found in many papers involving the catalytic performance of heterogeneous catalysts<sup>17,18,37</sup> towards cycloaddition of CO<sub>2</sub> with epoxides. In addition to ECH, the catalyst also exhibits good activities in the cases of ethylene oxide (EO), 1,2-butylene oxide (BO), styrene oxide (SO). Note: the isolated yields for EC, PC, and BC are appreciably lower than the values determined by GC, which is probably attributed to partial loss of products during separation and purification procedures. Nonetheless, using cyclohexene oxide as a substrate, the conversion is lower than 10%. This is mainly caused by the unique electronic environment of cyclohexene oxide, which hinders nucleophilic attack and thus reduces the ring-opening rate. In fact, in other catalyst systems reported previously<sup>19,22,60</sup>, the catalytic activities when using cyclohexene were much lower than EO, SO, etc.

**Table 3** Catalytic results for the cycloaddition reactions using various epoxides<sup>a</sup>.

Epoxide	Conv. (%)	Sel. (%)	Yield (%) <sup>b</sup>
	78	95	74 (68)
	55	95	52 (46)
	50	96	48 (35)
	88	94	82
	75	93	70
	<10	93	9

<sup>a</sup> Reaction conditions: 8 mL of PO, 2 mL of DMF,  $p(\text{CO}_2) = 2.0$  MPa,  $T = 140$  °C,  $t = 6$  h, and 0.2 g of ZnBr<sub>2</sub>/g-C<sub>3</sub>N<sub>4</sub>. <sup>b</sup> The values in the bracket are isolated yields.

**Table 4** summarizes the catalytic performances of various materials for the cycloaddition of CO<sub>2</sub> with PO. To the best of our knowledge, it covers almost all the g-C<sub>3</sub>N<sub>4</sub>-based materials reported recently. As shown in **Table 4**, the reaction temperatures are between 130 and 150 °C and in general, the CO<sub>2</sub> pressure are in the range of 2.0–3.5 MPa. Among these

materials, g-C<sub>3</sub>N<sub>4</sub>/SBA-15 and *n*-butBr/mp-C<sub>3</sub>N<sub>4</sub> exhibit the highest quasi-TOF values. Despite such high catalytic activities, it should be pointed out that the preparation of the two catalysts were very complicated. In the case of g-C<sub>3</sub>N<sub>4</sub>/SBA-15 material, it demanded mesoporous siliceous SBA-15 as a catalyst support, and was prepared by a chemical-vapor-deposition method. Furthermore, in the corresponding catalytic experiment, additional zinc halide was used as a co-catalyst to enhance its

catalytic performance. Also, *n*-butBr/mp-C<sub>3</sub>N<sub>4</sub> (as well as ZnBr<sub>2</sub>/mp-C<sub>3</sub>N<sub>4</sub> and MS-MCN) was prepared through a nanocasting approach using silica nanoparticles as hard template, where involved HF-etching procedure. Although the catalytic activity of ZnBr<sub>2</sub>/g-C<sub>3</sub>N<sub>4</sub> is moderate, the preparation of the catalyst is based on a simple impregnation method, requiring no additional template and therefore is more facile and eco-friendly than other catalysts described in **Table 4**.

**Table 4** Catalytic performances of various g-C<sub>3</sub>N<sub>4</sub>-based materials in cycloaddition of CO<sub>2</sub> with PO to PC.

Entry	Catalyst	<i>T</i> (°C)	<i>p</i> (CO <sub>2</sub> )(MPa)	<i>t</i> (h)	<i>V</i> <sub>PO</sub> (mL)	<i>W</i> <sub>cat.</sub> (mg)	Yield (%)	quasi-TOF (h <sup>-1</sup> ) <sup>g</sup>
1 <sup>a 37</sup>	MS-MCN	140	0.55	10	1.5	20	30.6	3.3
2 <sup>b 17</sup>	g-C <sub>3</sub> N <sub>4</sub> /SBA-15	150	3.5	1.5	3	100	96.1	28.1
3 <sup>c 39</sup>	<i>n</i> -butBr/mp-C <sub>3</sub> N <sub>4</sub>	140	2.5	6	10	200	87.7	10.7
4 <sup>d 38</sup>	ZnBr <sub>2</sub> /mp-C <sub>3</sub> N <sub>4</sub>	140	2.5	6	7	200	98.9	8.4
5 <sup>e 35</sup>	u-g-C <sub>3</sub> N <sub>4</sub> -480	130	2.0	4	1.5	50	23.7	2.6
6 <sup>f 40</sup>	g-C <sub>3</sub> N <sub>4</sub> -475-NaOH	140	2.0	6	10	400	89.5	5.4
7	ZnBr <sub>2</sub> /g-C <sub>3</sub> N <sub>4</sub>	140	2.0	6	8	200	52.0	5.1

<sup>a</sup> Prepared using disk-shaped 2D hexagonal mesoporous silica as a hard template and melamine as a precursor. <sup>b</sup> Prepared using SBA-15 as a catalytic support and dicyandiamide as a precursor through a chemical-vapor-deposition method. Zn<sup>2+</sup> was further doped into g-C<sub>3</sub>N<sub>4</sub>/SBA-15 as an additive. <sup>c</sup> Prepared using silica nanoparticles as hard templates and cyanamide as a precursor. The synthesized mp-C<sub>3</sub>N<sub>4</sub> was grafted with *n*-bromobutane. <sup>d</sup> ZnBr<sub>2</sub> supported on mp-C<sub>3</sub>N<sub>4</sub> material. <sup>e</sup> Prepared using urea as a starting material without addition of any template. <sup>f</sup> Synthesized by guanidine hydrochloride as a precursor treated by NaOH. <sup>g</sup> The detailed calculation method for quasi-TOF is expressed in the experimental section.

#### 4. Discussion

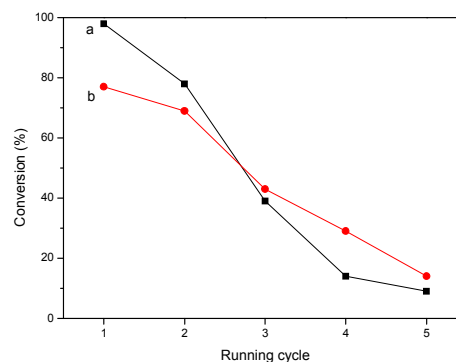
**Table 5** Catalytic results of catalysts prepared with various heating temperatures<sup>a</sup>.

Sample	Conv. (%)	Sel. (%)	Yield (%)
ZnBr <sub>2</sub> /g-C <sub>3</sub> N <sub>4</sub> -250	98	99	97
ZnBr <sub>2</sub> /g-C <sub>3</sub> N <sub>4</sub> -300	77	97	74
ZnBr <sub>2</sub> /g-C <sub>3</sub> N <sub>4</sub> -350	64	97	62
ZnBr <sub>2</sub> /g-C <sub>3</sub> N <sub>4</sub> -400	55	95	52
ZnBr <sub>2</sub> /g-C <sub>3</sub> N <sub>4</sub> -450	41	97	40
ZnBr <sub>2</sub> /g-C <sub>3</sub> N <sub>4</sub> -500	26	96	25

<sup>a</sup> Reaction conditions: 8 mL of PO, 2 mL of DMF, *p*(CO<sub>2</sub>) = 2.0 MPa, *W*<sub>cat.</sub> = 0.2 g, *T* = 140 °C, *t* = 6 h.

The present work reports synthesis of a series of zinc halides catalysts supported on g-C<sub>3</sub>N<sub>4</sub> support. The ZnX<sub>2</sub>/g-C<sub>3</sub>N<sub>4</sub> materials demonstrate catalysis towards the transformation of CO<sub>2</sub> to various cyclic carbonates. Wherein, the active sites of the catalysts are preliminarily supposed as zinc cation and halide. Furthermore, ZnBr<sub>2</sub>/g-C<sub>3</sub>N<sub>4</sub> exhibits superior catalytic activity to its two counterparts of zinc halide (Cl/I), also to other catalysts with single Zn or halogen component. The FT-IR and XPS profiles verify a potential complexing interaction between Zn and N of g-C<sub>3</sub>N<sub>4</sub>. In view of the catalytic and characterization results, we surmise that the complexing is possibly facilitated during its heating treatment of ZnX<sub>2</sub>/g-C<sub>3</sub>N<sub>4</sub>. With this in mind, we further examined the catalytic performances of a series of ZnBr<sub>2</sub>/g-C<sub>3</sub>N<sub>4</sub> materials prepared adopting various heating temperatures in range of 250 to 500 °C. Note, the nominal loading amount of ZnBr<sub>2</sub> for each sample is identical. As summarized in **Table 5**, it can be found that the temperature plays a significant role in determining the catalytic activity of ZnBr<sub>2</sub>/g-C<sub>3</sub>N<sub>4</sub>-*T* catalyst. Specifically, as the heating

temperature is increased, the catalytic conversion is decreased monotonously. The highest activity is offered by ZnBr<sub>2</sub>/g-C<sub>3</sub>N<sub>4</sub>-250, affording an outstanding PC yield up to 98%. However, it should be pointed out that the catalytic results in **Table 5** were all collected in the first catalytic run.



**Fig. 9** Recycling tests of cycloaddition reactions catalyzed by ZnBr<sub>2</sub>/g-C<sub>3</sub>N<sub>4</sub>-250 (a) and ZnBr<sub>2</sub>/g-C<sub>3</sub>N<sub>4</sub>-300 (b) samples. Reaction conditions: 8 mL of PO, 2 mL of DMF, *W*<sub>cat.</sub> = 0.2 g, *T* = 140 °C, *t* = 6 h. The selectivity to PC for each case is higher than 95%.

**Fig. 9** shows the catalytic performances of fresh and recycled ZnBr<sub>2</sub>/g-C<sub>3</sub>N<sub>4</sub>-250 and ZnBr<sub>2</sub>/g-C<sub>3</sub>N<sub>4</sub>-300 materials in the cycloaddition reactions. Surprisingly, the catalytic activity for each case descends sharply within the consecutive runs, and indeed, the PO conversions for the two catalysts subjected to five times of use are dropped to ca. 15%. As discussed above, the active sites for the catalytic cycloaddition are actually zinc cations and halides. In this regard, it can speculate that most of supported ZnBr<sub>2</sub> in ZnBr<sub>2</sub>/g-C<sub>3</sub>N<sub>4</sub>-250 and ZnBr<sub>2</sub>/g-C<sub>3</sub>N<sub>4</sub>-300 underwent severe leaching in their recycling experiments.



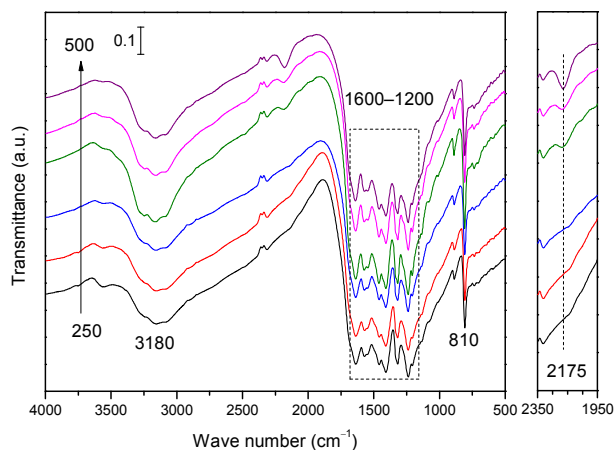


Fig. 10 FT-IR spectra of  $\text{ZnBr}_2/\text{g-C}_3\text{N}_4\text{-}T$  materials prepared under various heating temperatures.

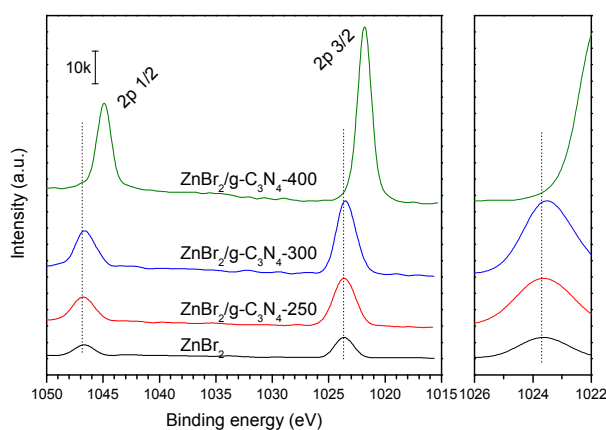


Fig. 11 Zn 2p XP spectra of the pure  $\text{ZnBr}_2$  and  $\text{ZnBr}_2/\text{g-C}_3\text{N}_4\text{-}T$  materials prepared under various heating temperatures.

In order to search out a reasonable reason explaining the drastic decline in terms of catalytic activity, the above three catalysts were then characterized by XPS and FT-IR spectroscopy. The difference in chemical functionalities of  $\text{ZnBr}_2/\text{g-C}_3\text{N}_4$  treated under various temperatures can be clearly displayed in the FT-IR spectra (Fig. 10). For the  $\text{ZnBr}_2/\text{g-C}_3\text{N}_4\text{-}T$  samples adopting lower temperature ( $T < 350^\circ\text{C}$ ), no bands associated with Zn-N (ca.  $2185\text{ cm}^{-1}$ ) is discovered<sup>46</sup>, suggesting that zinc has no interaction with nitrogen of  $\text{g-C}_3\text{N}_4$ , namely  $\text{ZnBr}_2$  exists in the free state on the surface of  $\text{g-C}_3\text{N}_4$ . Another proof is provided in the corresponding Zn 2p XP spectra. As shown in Fig. 11, the positions of the two primary signals acquired in the spectra of  $\text{ZnBr}_2/\text{g-C}_3\text{N}_4\text{-}250$  and  $\text{ZnBr}_2/\text{g-C}_3\text{N}_4\text{-}300$  are very close to that of the pure  $\text{ZnBr}_2$  sample. It is worth pointing out that the two peaks of  $\text{ZnBr}_2/\text{g-C}_3\text{N}_4\text{-}300$  are actually moved slightly to lower binding energy, suggesting that a small proportion of Zn is included in  $\text{g-C}_3\text{N}_4$  matrix<sup>46,54</sup>. However, in sharp contrast with  $\text{ZnBr}_2/\text{g-C}_3\text{N}_4\text{-}400$ , the detailed XP spectra could reasonably rule out the

complexing between Zn and N in the  $\text{ZnBr}_2/\text{g-C}_3\text{N}_4\text{-}250$  and  $\text{ZnBr}_2/\text{g-C}_3\text{N}_4\text{-}300$  materials. In brief, because of the low temperatures of heating treatment for  $\text{ZnBr}_2/\text{g-C}_3\text{N}_4$ , the interaction between  $\text{ZnBr}_2$  and  $\text{g-C}_3\text{N}_4$  is quite weak, or possibly in the form of physical adsorption. During the recycling tests, most of adsorbed  $\text{ZnBr}_2$  was dispersed and eventually leached into the liquid phase. After each rising step, the concentration of  $\text{ZnBr}_2$  available on the surface of  $\text{g-C}_3\text{N}_4$  becomes lower and lower, thereby responsible for the continuous decline of catalytic activity occurring in the two catalysts (Fig. 9).

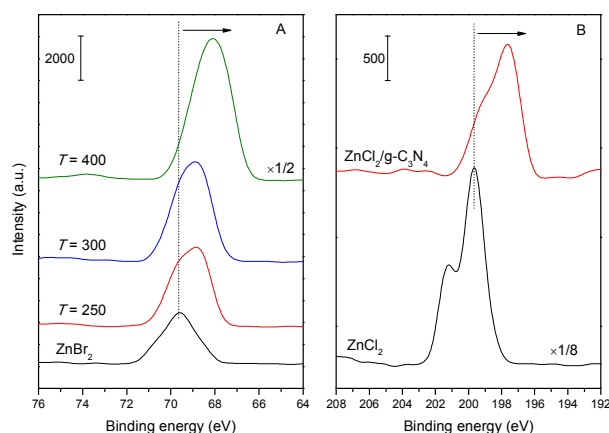
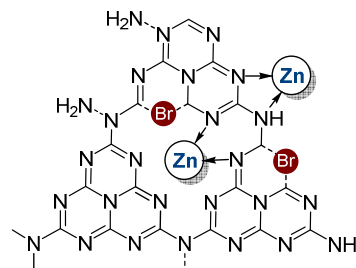


Fig. 12 XP spectra of Br 3d (A) and Cl 2p (B) region of the pure  $\text{ZnBr}_2$ ,  $\text{ZnCl}_2$ , and  $\text{ZnBr}_2/\text{g-C}_3\text{N}_4\text{-}T$  and  $\text{ZnCl}_2/\text{g-C}_3\text{N}_4$  materials.

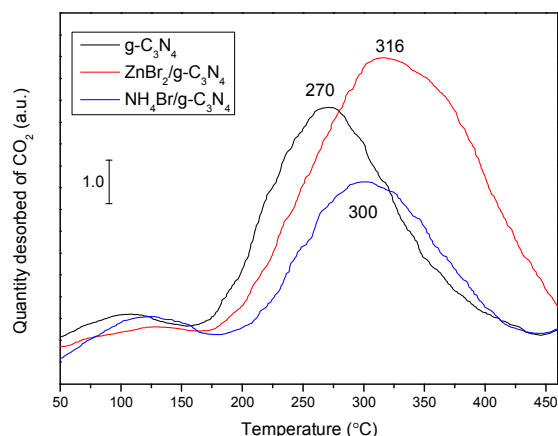


Scheme 1 A possible structure of  $\text{ZnBr}_2$  anchored in  $\text{g-C}_3\text{N}_4$  matrix.

The above findings inspire us to further elucidate the chemical bonding state of halogen in the  $\text{ZnX}_2/\text{g-C}_3\text{N}_4$  composites. Correspondingly, the detailed spectra of Br 3d and Cl 2p region of the materials were also recorded. The remarkable difference between  $\text{ZnX}_2/\text{g-C}_3\text{N}_4$  and their corresponding pure zinc halides can be found in Fig. 12. For the composite of  $\text{ZnX}_2/\text{g-C}_3\text{N}_4$ , both the position of Br 3d and Cl 2p signals evidences a pronounced shift towards lower binding energies, even identified in the spectrum of  $\text{ZnBr}_2/\text{g-C}_3\text{N}_4\text{-}250$  synthesized under a low heating temperature. This similar phenomenon has been also previously reported in the work involving iodine<sup>61</sup> or phosphorus-doped<sup>62</sup>  $\text{g-C}_3\text{N}_4$  materials, implying formation of the covalent bond between bromine/chlorine and  $\text{g-C}_3\text{N}_4$ . More specifically, the original  $\text{sp}^2$ -hybridized nitrogen in the tri-*s*-triazine units might be substituted by halogen in  $\text{ZnBr}_2/\text{g-C}_3\text{N}_4$ . However, the halogen

species are still negatively charged (inferred by **Fig. 12**) and simultaneously neutralized by zinc cations, as illustrated in **Scheme 1**.

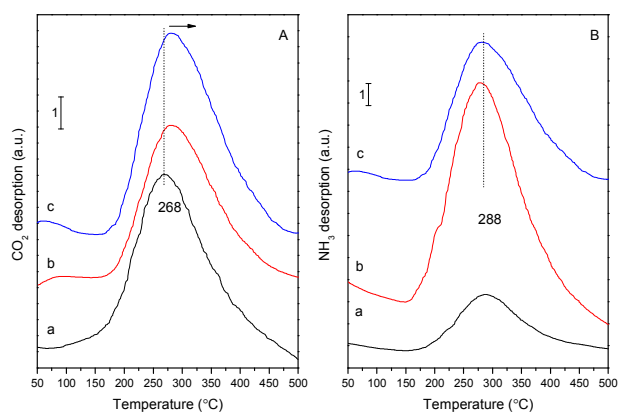
Since the bonding and existence of zinc and halogen elements have been comprehensively elucidated above, it is of interest to discuss the catalytic effect of  $ZnX_2$  in the catalytic reaction between  $CO_2$  with epoxides. Herein, we used PO as a representative probe molecule to perform a series of TPD measurements. As described in **Fig. 13**, the TPD profile of the pristine  $g-C_3N_4$  sample shows one major desorption peak of PO in the range of 200–430 °C (centered at ca. 270 °C). As for  $NH_4Br/g-C_3N_4$ , it is observed that the position of desorption peak is shifted to a higher temperature of ca. 300 °C, indicative of stronger adsorption of PO on the surface of  $NH_4Br/g-C_3N_4$  than the pristine  $g-C_3N_4$ . In sharp contrast, the TPD profile  $ZnBr_2/g-C_3N_4$  demonstrates a much higher desorption temperature; the peak is centered at ca. 316 °C, also accompanied with an apparent shoulder at ca. 350 °C. Undoubtedly, the desorption peak occurring at such high temperature is originated from the strong chemical adsorption. Additionally, judging from the three TPD curves, it is estimated that  $ZnBr_2/g-C_3N_4$  has superior desorption quantity of PO to  $g-C_3N_4$  and  $NH_4Br/g-C_3N_4$ . Based on the differences of the three materials in terms of desorption temperature and quantity, we can infer that  $ZnBr_2$  is a key component in adsorbing epoxide on the surface of catalyst and more importantly, the combination of zinc and halide could enhance the adsorbing capacity.



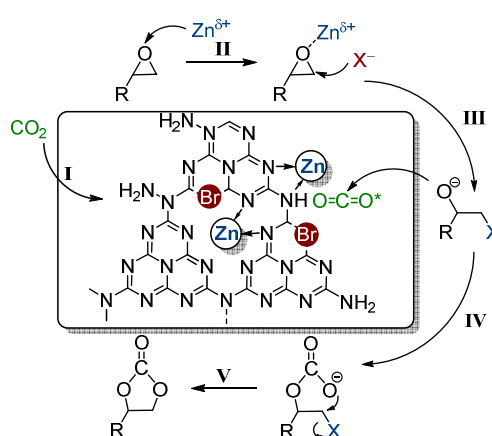
**Fig. 13** PO-TPD profiles of various catalysts.

In order to verify possible change of acidity and basicity of  $g-C_3N_4$  before and after the introduction of  $ZnX_2$ ,  $CO_2$ -TPD and  $NH_3$ -TPD experiments were performed. The pure and loaded  $g-C_3N_4$  materials exhibit major desorption peaks of  $CO_2$  in the range of 75–500 °C (**Fig. 14A**), suggesting that the materials possess typical basic sites on their surface. The desorption peak gained in the pure  $g-C_3N_4$  is centered at 268 °C, corresponding to chemical adsorption of  $CO_2$  by the weak basic sites<sup>34,63</sup>. Upon loading  $ZnO$  and  $ZnBr_2$ , the peaks are moved to higher temperatures, indicative of enhanced basic strength in the supported  $g-C_3N_4$  composites. In our previous study<sup>34</sup>, we

reported that doping of a certain amount of  $Zn$  cation would lead to formation of more tertiary amines on the graphitic sheets of  $g-C_3N_4$ , consequently improving the overall basic intensity of  $g-C_3N_4$ . Given the explanation, it is reasonable to infer that the dopant of  $Zn$  cation into  $g-C_3N_4$  favors the adsorption of acidic  $CO_2$  molecules, which is responsible for their higher catalytic activities in cycloaddition of  $CO_2$  than the bare  $g-C_3N_4$  (**Table 2**). On the other hand, it is of surprise that the corresponding  $NH_3$ -TPD profiles (**Fig. 14B**) reveal the existence of a small amount of acidic sites on  $g-C_3N_4$ . We conjecture that the desorption signals might originate from the small ammonia-like molecules adsorbed on the surface of  $g-C_3N_4$  due to uncompleted condensation<sup>27</sup>. In the cases of  $ZnO/g-C_3N_4$  and  $ZnBr_2/g-C_3N_4$ , the dopant of  $Zn^{2+}$  species as classical Lewis acids, effectively strengthens the acidity of  $g-C_3N_4$ .



**Fig. 14**  $CO_2$ -TPD (A) and  $NH_3$ -TPD (B) profiles of  $g-C_3N_4$  (a),  $ZnO/g-C_3N_4$  (b), and  $ZnBr_2/g-C_3N_4$  (c) materials.



**Scheme 2** A possible reaction mechanism of cycloaddition of  $CO_2$  with PO catalyzed by  $ZnX_2/g-C_3N_4$ .

Herein, according to the aforementioned characterization results in this work and the relevant papers published previously<sup>16,21,38,56</sup>, a possible reaction pathway catalyzed by  $ZnBr_2/g-C_3N_4$  materials was proposed (**Scheme 2**). As noted above, the principle catalysis for the reaction between  $CO_2$  and

epoxides lies on both activation of CO<sub>2</sub> and ring-opening of epoxides. Owing to its abundant basic sites in forms of amino group, CO<sub>2</sub> molecules were initially adsorbed and then activated by g-C<sub>3</sub>N<sub>4</sub>. In addition, the basic solvent of DMF also contributes to the activation step. As for epoxide, zinc cations coordinate with the oxygen of epoxide, leading to polarization of C–O bonds thereof and meanwhile, the halide anions nucleophilically attack the less bulky carbon atoms of epoxide. Among the three halide anions (Cl<sup>−</sup>/Br<sup>−</sup>/I<sup>−</sup>), Cl<sup>−</sup> and I<sup>−</sup> own the highest nucleophilic and leaving abilities<sup>21,64</sup>, respectively. In comparison, Br<sup>−</sup> has more suitable capability in nucleophilically attacking and leaving, reasonably explaining its superior catalytic activity in the cycloaddition reaction to its counterparts (**Table 1**). The dual steps initiated by ZnX<sub>2</sub> accelerate the ring-opening of epoxide, yielding haloalkoxy anion. Subsequently, the haloalkoxy intermediate attacks the active CO<sub>2</sub> molecule attached on the surface of g-C<sub>3</sub>N<sub>4</sub> and thus transforms into a linear halocarbonate. Afterwards, the halocarbonate closes its ring by the leaving of halogen anion, and eventually turns into cyclic carbonate. At this juncture, it can be further clarified that the activation processes of CO<sub>2</sub> and epoxide are primarily achieved by g-C<sub>3</sub>N<sub>4</sub> and ZnX<sub>2</sub>. However, it should be stressed that, far more than a solid base, g-C<sub>3</sub>N<sub>4</sub> acts a significant role in loading the catalytic active species of ZnX<sub>2</sub>. As illuminated above, through the formation of Zn–N complex together with the insertion of halogen into g-C<sub>3</sub>N<sub>4</sub> matrix, the g-C<sub>3</sub>N<sub>4</sub> support steadily anchors and immobilizes ZnX<sub>2</sub> species on its surface, and thus restrains the loss of ZnX<sub>2</sub> into liquid phase, consequently realizing heterogeneous catalysts.

## 5. Conclusion

In summary, a series of ZnX<sub>2</sub>/g-C<sub>3</sub>N<sub>4</sub> composites have been fabricated by a simple preparation approach. The temperature of heating treatment has a significant effect on the bonding states of Zn and halogen species. Under optimized conditions, zinc can be coordinated with nitrogen atoms of g-C<sub>3</sub>N<sub>4</sub> while halogen substitutes the nitrogen atoms in the framework of g-C<sub>3</sub>N<sub>4</sub>. Among various catalysts, ZnBr<sub>2</sub>/g-C<sub>3</sub>N<sub>4</sub> demonstrates the highest activity in cycloaddition of CO<sub>2</sub> with PO. The catalysts could be reused for at least five times and show wide applicability for other cycloaddition reactions with various epoxides. Zinc halide are confirmed as a key component in activating epoxide while g-C<sub>3</sub>N<sub>4</sub> not only serves as a solid base to activate CO<sub>2</sub> but also plays a vital role in anchoring and immobilizing zinc halide on the surface of g-C<sub>3</sub>N<sub>4</sub>. We think that the findings could provide a comprehensive insight of the support effect of g-C<sub>3</sub>N<sub>4</sub> for zinc halides and other wide metal halides, and constitute a new strategy for designing more novel heterogeneous metal-halide-based catalysts.

## Conflicts of interest

There are no conflicts to declare.

## Acknowledgements

The work was financially supported by PetroChina Innovation Foundation (2018D-5007-0508), Advanced Catalysis and Green Manufacturing Collaborative Innovation Centre (ACGM2016-06-28), Foundation of State Key Laboratory of High-efficiency Utilization of Coal and Green Chemical Engineering (2017-K28), Foundation of State Key Laboratory of Chemical Resource Engineering (CRE-2017-C-109), and the Top-notch Academic Programs Project of Jiangsu Higher Education Institutions (PPZY2015B145). J. Xu also thanks Jun-Jing Ding of Shiyanjia Lab for his help in XPS characterization.

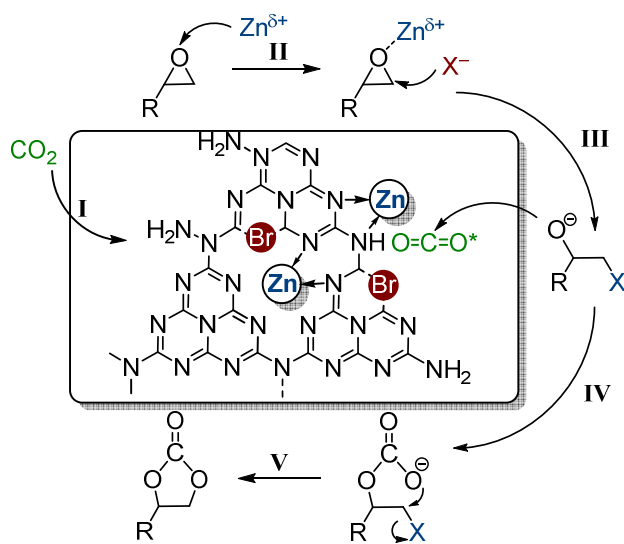
## Notes and references

1. L. Wang, G. Zhang, K. Kodama and T. Hirose, *Green Chem.*, 2016, **18**, 1229-1233.
2. J. Roeser, K. Kailasam and A. Thomas, *ChemSusChem*, 2012, **5**, 1793-1799.
3. M. North, R. Pasquale and C. Young, *Green Chem.*, 2010, **12**, 1514-1539.
4. J. Peng, H.-J. Yang, N. Song and C.-Y. Guo, *J. CO<sub>2</sub> Util.*, 2015, **9**, 16-22.
5. D. Ma, H. Zheng, H.-M. Wan, Y. Chen, J. Xu and B. Xue, *Micropor. Mesopor. Mater.*, 2018, **258**, 244-250.
6. D.-H. Lan, N. Fan, Y. Wang, X. Gao, P. Zhang, L. Chen, C.-T. Au and S.-F. Yin, *Chin. J. Catal.*, 2016, **37**, 826-845.
7. R. A. Watile, K. M. Deshmukh, K. P. Dhake and B. M. Bhanage, *Catal. Sci. Technol.*, 2012, **2**, 1051-1055.
8. J. N. Appaturi and F. Adam, *Appl. Catal. B*, 2013, **136-137**, 150-159.
9. L. Han, H. Li, S.-J. Choi, M.-S. Park, S.-M. Lee, Y.-J. Kim and D.-W. Park, *Appl. Catal. A*, 2012, **429**, 67-72.
10. J. K. Lee, Y. J. Kim, Y. Choi, H. Lee, J. S. Lee, J. Hong, E. Jeong, H. S. Kim and M. Cheong, *Appl. Catal. B*, 2012, **111-112**, 621-627.
11. Y. Xie, T. T. Wang, X. H. Liu, K. Zou and W. Q. Deng, *Nat. Commun.*, 2013, **4**, 1960.
12. J. Peng, H.-J. Yang, S. Wang, B. Ban, Z. Wei, B. Lei and C.-Y. Guo, *J. CO<sub>2</sub> Util.*, 2018, **24**, 1-9.
13. J. He, T. Wu, Z. Zhang, K. Ding, B. Han, Y. Xie, T. Jiang and Z. Liu, *Chem. -Eur. J.*, 2007, **13**, 6992-6997.
14. J. Langanke, L. Greiner and W. Leitner, *Green Chem.*, 2013, **15**, 1173-1182.
15. W.-L. Dai, S.-L. Luo, S.-F. Yin and C.-T. Au, *Appl. Catal. A*, 2009, **366**, 2-12.
16. J. Sun, L. Wang, S. Zhang, Z. Li, X. Zhang, W. Dai and R. Mori, *J. Mol. Catal. A*, 2006, **256**, 295-300.
17. Z. Huang, F. Li, B. Chen, T. Lu, Y. Yuan and G. Yuan, *Appl. Catal. B*, 2013, **136**, 269-277.
18. J. Zhu, T. Diao, W. Wang, X. Xu, X. Sun, S. A. C. Carabineiro and Z. Zhao, *Appl. Catal. B*, 2017, **219**, 92-100.
19. R. R. Kuruppathparambil, T. Jose, R. Babu, G. Hwang, A. C. Kathalikkattil, D. Kim and D. Park, *Appl. Catal. B*, 2016, **182**, 562-569.
20. L. Wang, K. Kodama and T. Hirose, *Catal. Sci. Technol.*, 2016, **6**, 3872-3877.
21. M. Liu, B. Liu, L. Shi, F. Wang, L. Liang and J. Sun, *RSC Adv.*, 2015, **5**, 960-966.
22. M. Liu, K. Gao, L. Liang, J. Sun, L. Sheng and M. Arai, *Catal. Sci. Technol.*, 2016, **6**, 6406-6416.
23. S.-S. Wu, X.-W. Zhang, W.-L. Dai, S.-F. Yin, W.-S. Li, Y.-Q. Ren and C.-T. Au, *Appl. Catal. A*, 2008, **341**, 106-111.
24. Y. Wang, X. Wang and M. Antonietti, *Angew. Chem. Int. Ed.*,

- 2012, **51**, 68-89.
25. X. Wang, X. Chen, A. Thomas, X. Fu and M. Antonietti, *Adv. Mater.*, 2009, **21**, 1609-1612.
26. S. Cao, J. Low, J. Yu and M. Jaroniec, *Adv. Mater.*, 2015, **27**, 2150-2176.
27. J. Zhu, P. Xiao, H. Li and S. A. C. Carabineiro, *ACS Appl. Mater. Inter.*, 2014, **6**, 16449-16465.
28. J. Ding, Q. Liu, Z. Zhang, X. Liu, J. Zhao, S. Cheng, B. Zong and W.-L. Dai, *Appl. Catal. B*, 2015, **165**, 511-518.
29. J. Xu, Y. Chen, Y. Hong, H. Zheng, D. Ma, B. Xue and Y.-X. Li, *Appl. Catal. A*, 2018, **549**, 31-39.
30. K. S. Lakhi, D. Park, K. Albahily, W. Cha, B. Viswanathan, J. Choy and A. Vinu, *Chem. Soc. Rev.*, 2016, **46**, 72-101.
31. Y. Zheng, J. Liu, J. Liang, M. Jaroniec and S. Z. Qiao, *Energy Environ. Sci.*, 2012, **5**, 6717-6731.
32. F. Goettmann, A. Fischer, M. Antonietti and A. Thomas, *Angew. Chem. Int. Ed.*, 2006, **45**, 4467-4471.
33. A. Thomas, A. Fischer, F. Goettmann, M. Antonietti, J.-O. Müller, R. Schlögl and J. M. Carlsson, *J. Mater. Chem.*, 2008, **18**, 4893-4908.
34. J. Xu, K.-Z. Long, Y. Wang, B. Xue and Y.-X. Li, *Appl. Catal. A*, 2015, **496**, 1-8.
35. Q. Su, J. Sun, J. Wang, Z. Yang, W. Cheng and S. Zhang, *Catal. Sci. Technol.*, 2014, **4**, 1556-1562.
36. F. Goettmann, A. Thomas and M. Antonietti, *Angew. Chem. Int. Ed.*, 2007, **46**, 2717-2720.
37. M. B. Ansari, B.-H. Min, Y.-H. Mo and S.-E. Park, *Green Chem.*, 2011, **13**, 1416-1421.
38. J. Xu, F. Wu, Q. Jiang, J.-K. Shang and Y.-X. Li, *J. Mol. Catal. A*, 2015, **403**, 77-83.
39. J. Xu, F. Wu, Q. Jiang and Y.-X. Li, *Catal. Sci. Technol.*, 2015, **5**, 447-454.
40. J. Xu, J.-K. Shang, Q. Jiang, Y. Wang and Y.-X. Li, *RSC Adv.*, 2016, **6**, 55382-55392.
41. Z. Huang, F. Li, B. Chen and G. Yuan, *Catal. Sci. Technol.*, 2016, **6**, 2942-2948.
42. Z. Ding, X. Chen, M. Antonietti and X. Wang, *ChemSusChem*, 2011, **4**, 274-281.
43. K. K. R. Datta, B. V. S. Reddy, K. Ariga and A. Vinu, *Angew. Chem. Int. Ed.*, 2010, **49**, 5961-5965.
44. B. Xue, Y. Chen, Y. Hong, D.-Y. Ma, J. Xu and Y.-X. Li, *Chin. J. Catal.*, 2018, **39**, 1263-1271.
45. Z. Chen, J. Zhang, S. Zheng, J. Ding, J. Sun, M. Dong, M. Abbas, Y. Chen, Z. Jiang and J. Chen, *Mol. Catal.*, 2018, **444**, 90-99.
46. B. Yue, Q. Li, H. Iwai, T. Kako and J. Ye, *Sci. Technol. Adv. Mater.*, 2011, **12**, 034401.
47. L. Muniandy, F. Adam, A. R. Mohamed, A. Iqbal and N. R. A. Rahman, *Appl. Sur. Sci.*, 2017, **398**, 43-55.
48. M. J. Bojdys, J.-O. Müller, M. Antonietti and A. Thomas, *Chem. - Eur. J.*, 2008, **14**, 8177-8182.
49. Y. Guo, T. Chen, Q. Liu, Z. Zhang and X. Fang, *J. Phys. Chem. C*, 2016, **120**, 25328-25337.
50. Y. Wang, Q. Jiang, J.-K. Shang, J. Xu and Y.-X. Li, *Acta Phys. -Chim. Sin.*, 2016, **32**, 1913-1928.
51. F. Dong, L. Wu, Y. Sun, M. Fu, Z. Wu and S. C. Lee, *J. Mater. Chem.*, 2011, **21**, 15171-15174.
52. J. Zhu, Y. Wei, W. Chen, Z. Zhao and A. Thomas, *Chem. Commun.*, 2010, **46**, 6965-6967.
53. Y. Lu, F. Yu, J. Hu and J. Liu, *Appl. Catal. A*, 2012, **429-430**, 48-58.
54. J. Wang, F. Su and W. Zhang, *J. Solid State Electrochem.*, 2014, **18**, 2921-2929.
55. M. C. Biesinger, L. W. M. Lau, A. R. Gerson and R. S. C. Smart, *Appl. Sur. Sci.*, 2010, **257**, 887-898.
56. S. Zhong, L. Liang, B. Liu and J. Sun, *J. CO2 Util.*, 2014, **6**, 75-79.
57. L. Wang, L. Lin, G. Zhang, K. Kodama, M. Yasutake and T. Hirose, *Chem. Commun.*, 2014, **50**, 14813-14816.
58. W.-L. Dai, B. Jin, S.-L. Luo, S.-F. Yin, X.-B. Luo and C.-T. Au, *J. CO2 Util.*, 2013, **3-4**, 7-13.
59. L.-F. Xiao, F.-W. Li, J.-J. Peng and C.-G. Xia, *J. Mol. Catal. A*, 2006, **253**, 265-269.
60. J. Sun, W. Cheng, W. Fan, Y. Wang, Z. Meng and S. Zhang, *Catal. Today*, 2009, **148**, 361-367.
61. G. Zhang, M. Zhang, X. Ye, X. Qiu, S. Lin and X. Wang, *Adv. Mater.*, 2014, **26**, 805-809.
62. Y. Zhang, T. Mori, J. Ye and M. Antonietti, *J. Am. Chem. Soc.*, 2010, **132**, 6294-6295.
63. N. D. Shcherban, P. Mäki-Arvela, A. Aho, S. A. Serghiienko, P. S. Yaremov, K. Eränen and D. Y. Murzin, *Catal. Sci. Technol.*, 2018, **8**, 2928-2937.
64. W. Cheng, X. Chen, J. Sun, J. Wang and S. Zhang, *Catal. Today*, 2013, **200**, 117-124.



## Graphical Abstract



Zinc halides are anchored on g-C<sub>3</sub>N<sub>4</sub> support and efficiently catalyze cycloaddition of CO<sub>2</sub> with epoxides to cyclic carbonates.